DeepSpec: a Broad-band $\mathcal{R} \sim 650$ Spectrograph with Multiplexing Capabilities

Irani I.[a], Ben-Ami, S.[a], Sofer-Rimalt, Y.[a], Ofek, E. O. [a], Mikhnevich, G.[a], Gal-Yam, A.[a], Achren, J.[b], Bichkovsky, A.[a], Blumenweig, A.[a], Hallakoun, N.[a], Hershko,O.[a], Kuncarayakti, H.[c,d], Mattila, S.[c], Ironi, O[a], Polishook, D.[a], and Yaron, O.[a]

[a]Department of Particle Physics and Astrophysics, Weizmann Institute of Science, 234 Herzl St, 7610001 Rehovot, Israel
[b]Incident Angle Oy, Capsiankatu 4 A 29, FI-20320 Turku, Finland
[c]Tuorla observatory, Department of Physics and Astronomy, University of Turku, Väisäläntie 20, 21500 Piikkiö, Finland
[d]Finnish Centre for Astronomy with ESO (FINCA), FI-20014 University of Turku, Finland

ABSTRACT

DeepSpec is a novel $\mathcal{R} \sim 650$ broad-band (365nm-900nm) spectrograph for the Weizmann Multi-Aperture Spectroscopic Telescope (MAST), an array of 20×61 cm prime focus telescopes dedicated for spectroscopic observations, at the Weizmann astronomical observatory in Israel. MAST/DeepSpec is capable of either acting as a single 2.7m telescope or multiplexing over the entire sky using smaller flexible groups. This approach will make the combination of MAST/DeepSpec a unique facility worldwide in terms of its low cost, flexibility, and efficiency, capable of observing up to hundreds of targets per night spread over large areas. With an end-to-end throughput of $> 65\%$, DeepSpec will be able to observe targets fainter than 20 mag in a 15-min exposure using all telescopes, or tens/hundreds of spectra per hour of 18-19 magnitude targets using smaller groups of telescopes – making it an ideal instrument for time-domain astronomy. All optics and hardware have been delivered during fall 2023 and DeepSpec is currently in the assembly, integration, and testing phase. It is planned to start on-sky commissioning in late summer 2024.

Keywords: Optical spectrographs, Telescope arrays

1. INTRODUCTION

In the era of wide-field surveys, spectroscopically classifying the increasing volumes of newly detected transients is becoming a considerable challenge. In addition to existing surveys such as the Zwicky transient facility (ZTF; 1), upcoming high-cadence surveys such as *ULTRASAT*(2), and Large Array Survey Telescope (LAST;3) will further increase the nightly volumes of detected fast transients and young supernovae. By providing extremely high cadence ($\sim$ 5 min) observations, *ULTRASAT* will allow us to study the very first photons emitted from SNe explosions – shock breakout, expected to peak in ultraviolet (UV) wavelengths. *ULTRASAT* is expected to observe tens of shock breakout signatures and hundreds of SNe in the first few days of their evolution (2), of which $\gtrsim 50\%$ will exhibit narrow "flash features" from early circumstellar material interaction (4). LAST is a new wide-field array currently under construction in the Weizmann Astronomical Observatory (WAO) located at the Kibbutz Neot Semadar in the Negev desert (3). LAST is comprised of an array of 48, 27-cm f/2.2 telescopes. The combined LAST array has a field of view (FOV) of 355 $\deg^2$, and will perform a survey with a cadence of $\sim$ 8 exposures per night over an area of 1500 $\deg^2$, and a lower cadence survey on 2500 $\deg^2$ with a limiting magnitude of 21 mag. It is expected to detect more than hundreds of SNe per year, alongside gamma-ray bursts, kilonovae, and other targets of opportunity.

Acquiring spectroscopic follow-up for the most interesting targets of these transient surveys requires significant spectroscopic resources from dedicated follow-up instruments. This is evidenced by the success of Spectral energy

Send correspondence to idoirani@gmail.com

distribution machined (SEDM; 5) on the P60 telescope, a robotic 60-inch that dedicates its entire time to ZTF transient follow-up. At the time of writing this paper, over 34% of supernovae classified on the Transient Name Server (TNS) are classified by SEDM*. A similar approach is needed for the LAST and *ULTRASAT* surveys, both probing a significantly larger volume compared to ZTF (3).

The Multi-Aperture Spectroscopic Telescope (MAST; Ben-Ami et al., in preparation) array adopt the distributed small telescope approach (e.g., 6) to the spectroscopic domain. It consists of a network of 20×61 cm F/3 prime focus parabolic telescopes from PlaneWave instruments. Each telescope will have an independent guiding and tracking system, feeding the target source into a 25/30 μm Few-Mode (FM) fused silica broad-spectrum fibers. Each telescope feeds 2 fibers - one for the science fiber and one for sky background. The fibers will channel light from each telescope to one of two instruments: (i) DeepSpec - a low spectral resolution broadband spectrograph; (ii) HighSpec: a high-resolution narrow band spectrograph. The incoming fibers from the telescope array will comprise a single long slit on the object plane and imaged to separate traces on the DeepSpec/HighSpec detectors (7; 8). DeepSpec is a high throughput ($> 65\%$), low-resolution ($\mathcal{R} \sim 650$) optical-NIR (365nm-900nm) spectrograph. In the following section, we describe the optical design of DeepSpec, the tolerancing process, and the expected performance of DeepSpec mounted on the full MAST array. Table 1 summarizes some basic properties of the WAO observatory and the custom PlaneWave telescopes used for MAST.

2. OPTICAL DESIGN

2.1 Overview

DeepSpec is designed to classify explosive transient events and filter through large samples of stellar objects. We therefore set the requirements according to the following list:

- A minimum spectral resolution $\mathcal{R} > 300$ ($v < 1000$ kms^{-1}) is required to discriminate high-ionization CSM features from broad ejecta features in SNe, and to improve upon the spectral resolution of SEDM.
- DeepSpec is required to reach an SNR of 10 with a 1500 s integration for a target at the limiting magnitude of the LAST survey (21 mag) at ideal conditions. This will allow us to identify rising targets and characterize them without using additional spectral resources.
- There are 45 fibers coming from the MAST array - 1 target and 1 sky fiber from each telescope, and 5 more fibers from the calibration unit (9). These combine to form a 5 mm long slit. Thus the collimator optics of DeepSpec are required to have a constant image quality over a 5 mm FOV. Similarly, the camera optics are required to have a FOV of at least 6 mm or the maximal trace length on the detector.
- DeepSpec is required to have a bandpass of 365nm-900nm. On the blue end, DeepSpec is required to cover both the Ca H&K lines and several high ionization C/O lines recently observed for exotic supernovae (e.g., 10; 11; 12.) On the red end, DeepSpec is required to cover the Ca IR triplet, important both for the observations of nebular spectra of SNe (12; 13) and for identifying white dwarf stars with gaseous debris disks (14).

A four-arm single prism-based design was found to satisfy all of the above requirements. We favored a prism-based design for the high throughput of its elements. Single rather than compound prisms were chosen to allow for a higher resolution for the same glass thickness, at the cost of a resolution curve that varies more over the transmitted bandpass. We chose to divide the band into four channels to preserve a relatively flat resolution curve, varying by $\mathcal{R}_{max}/\mathcal{R}_{min} \sim 1.5$ while covering the full bandwidth. Table 2 summarizes some basic properties of the DeepSpec spectrograph. Fig. 1 shows the optical layout of the system. Following a common path collimator, the beam is split by a set of dichroic mirrors into four bands, each dispersed by a minimum deviation prism and imaged by an achromat lens onto a separate detector, all optimized for the specific bandpass they operate in. High throughput over the instrument bandpass was prioritized in selecting the optical element glasses, bonding agent, and coatings. In Fig. 2, we show the total fiber to e^- efficiency, with a typical value of 70%, making DeepSpec one of the most efficient spectrographs of its kind (15; 16). In addition to the values in this figure,

*https://www.wis-tns.org/stats-maps

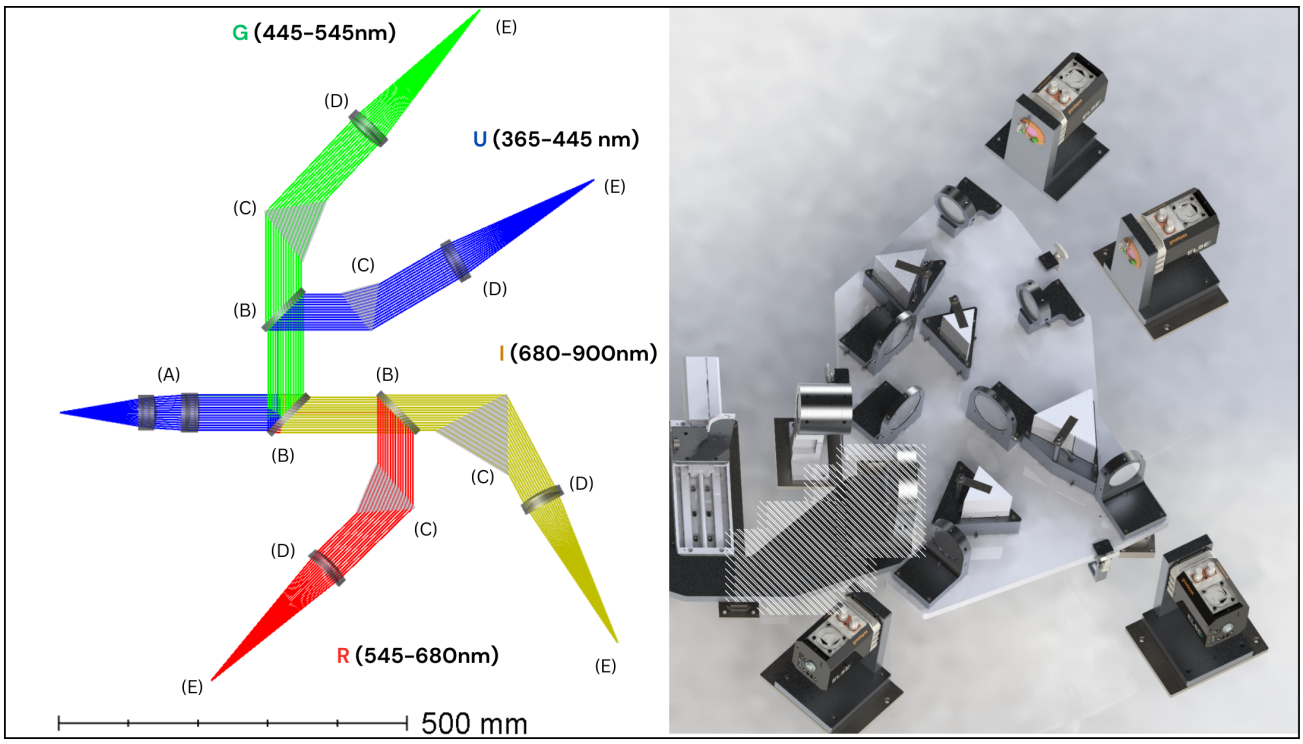

Figure 1. On the left, an optical system layout of DeepSpec: (S) source; (A) collimator lens; (B) dichroic; (C) prism; (D) camera lens; (E) Detector. On the right, a 3D rendering of the full system including opto-mechanics. A part of the HighSpec collimator (unrelated to the system discussed here) is marked with a hatch pattern.

telescope reflectivity losses ($> 85\%$) and fiber losses due to focal ratio degradation (FRD; 6%) and reflection losses on the fiber ends (8%) bring the total sky-to-e^- efficiency to 50%.

Table 1. Telescope and observatory parameters

Single unit effective diameter (mm)	580
Telescope Mirror reflectivity[a] (%)	> 85
Telescope focal length (mm)	1830
Number of units	20
Fiber core size (μm)	25
Maximum fiber throughput (reflectivity and FRD)[%]	86
Dark time Sky brightness [mag arcsec^{-2}]	20.9
Typical seeing [″]	1,4

2.2 Fiber feed

All fibers from the MAST telescopes, as well as fibers from the calibration system, are combined into a long-slit on a dedicated module, see Fig. 3. The module is mounted on a Zaber LRQ300AL linear stage for transitioning between DeepSpec and HighSpec, so that the fiber facets can be positions in each of the two spectrographs collimator focal point, see Fig. 3 bottom panel. This stage is the only moving part in the instrument side of the MAST array.

2.3 Collimator

The DeepSpec collimator is the only common path element in the DeepSpec design. Due to the broad bandpass of DeepSpec, a transmissive collimator is challenged by the need to maintain a high image quality over a wide

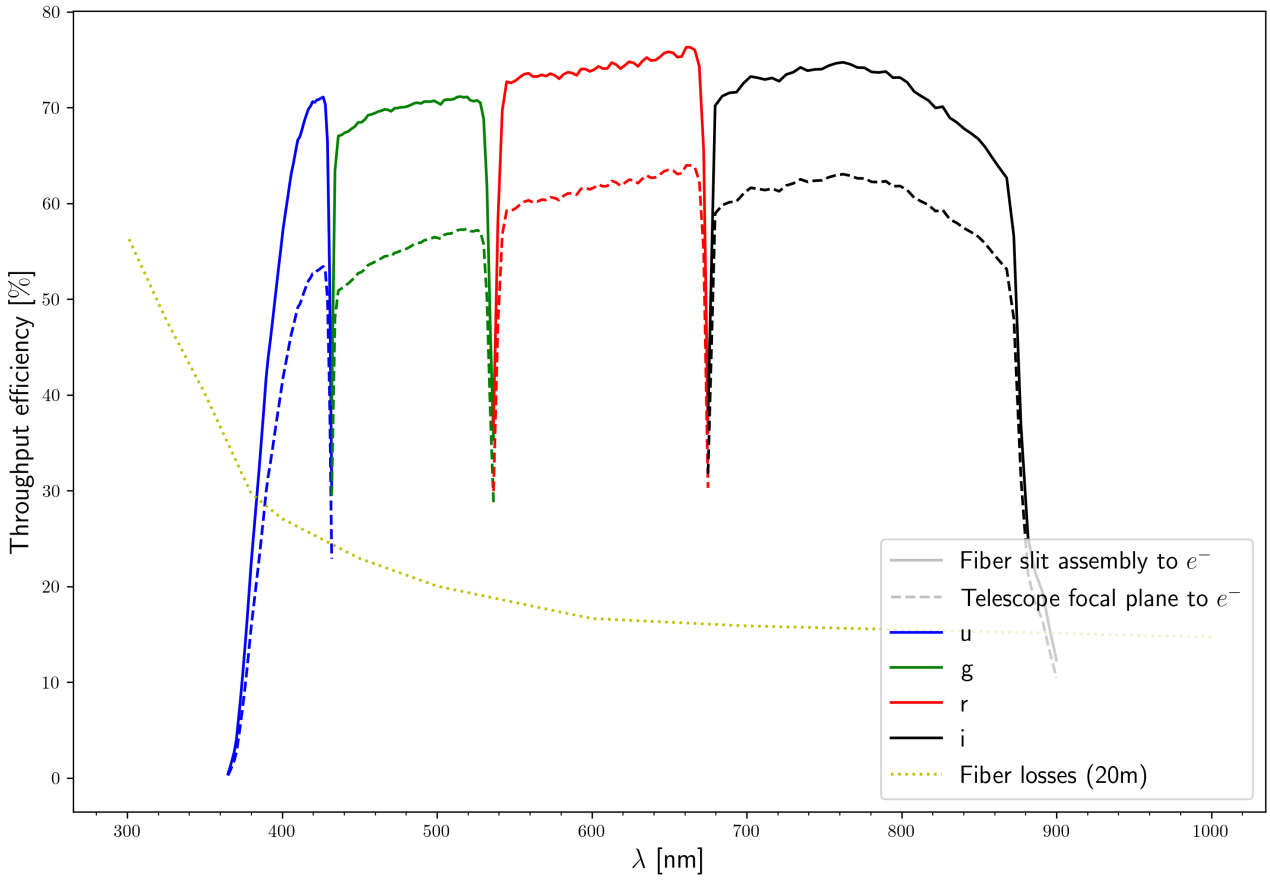

Figure 2. Total as-built throughput efficiency. Solid lines represent the slit to e^- throughput efficiency, including reflection losses (dichroics and coatings), transmission losses (dichroic mirrors, optical glasses, and bonding agents) and CCD quantum efficiency. The yellow dotted line represents the fiber losses (reflection, FRD, and propagation losses for a 20m fiber length). The blue, green red and black dashed curves show the total as build focal plane-to-electron conversion efficiency for DeepSpec on MAST.

field of view (covering the entire 5mm slit) over broad wavelength range. Indeed, when designing the DeepSpec collimator the leading aberration was chromatic, and a dual triplet design, similar to a Sonnar lens, was needed to achieve a high image quality of less than 10 μm. The tolerance requirements of this design proved challenging. In order to maintain image quality, relative partial dispersion between all wavelength had to be known to better than 0.3%. This requires the refractive index to be known to better than 10^{-5} accuracy, better than the catalog data accuracy data provided by most optical glass vendors. Thus, specific melt data for the glass batch used were needed. Once the optical glasses were purchased, refractive indices were acquired of 10 lines spanning the spectrograph bandpass for all collimator glasses. The radii of curvature for various elements was then re-optimized with the following procedure. First, We created a simulated set of glasses. Assuming refractive index measurements were independent, we drew 100 random realizations and calculated their abbe number ν_d. For each glass the simulated melt data for the 10th, 50th and 90th percentiles in Abbe number was save and input to Zemax Optics Studio. We then selected 16 combinations of glasses and simultaneously optimized the radii to provide good image quality for all combinations. While the resulting image quality was slightly worse than the optimized quality for the nominal model, it was significantly less sensitive to the expect variations in the index of refraction. We provide a full prescription of our collimator lenses in Table 3. At the time of writing this report, the DeepSpec collimator has been assembled and subject to preliminary testing. Our preliminary results indicate that we achieve nominal image quality over the entire field of view and bandpass.

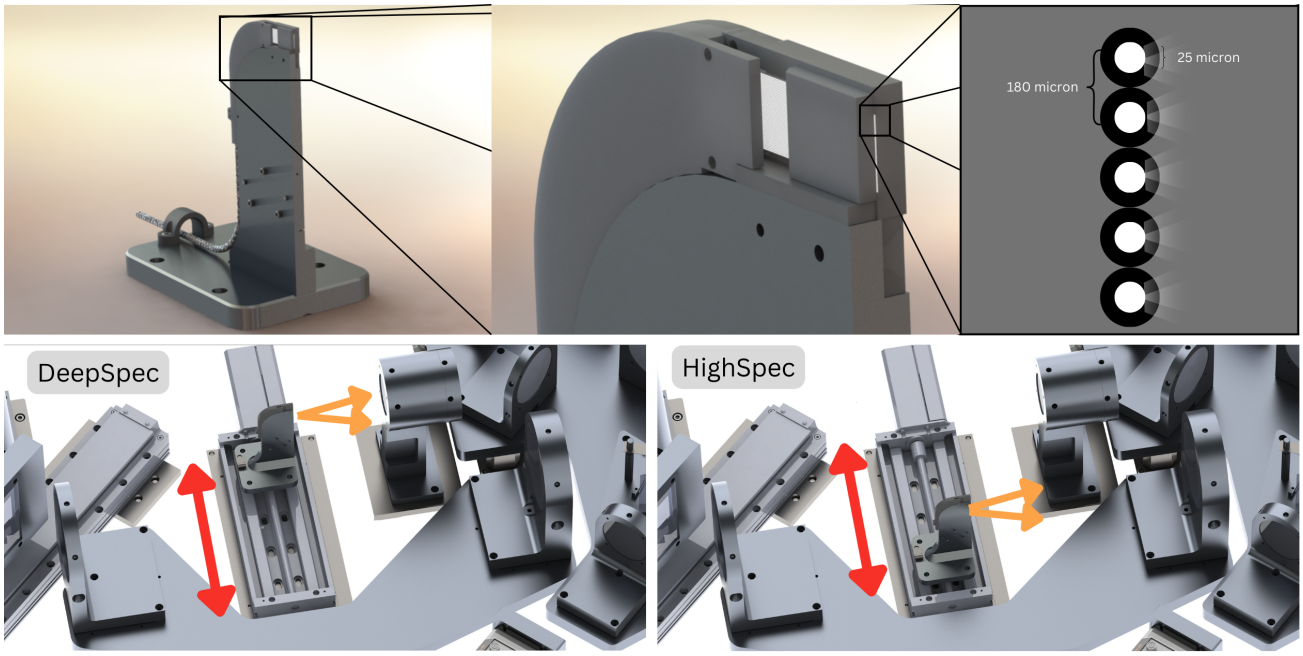

Figure 3. Top: A 3D rendering of the MAST Fiber feed assembly, serving as a long-slit input to the DeepSpec and HighSpec spectrographs. Each fiber core has a diameter of $25\mu m$, a center to center distance of $110\mu m$. Each of the 20 MAST telescopes sends one source and one background fibers to the spectrograph. In addition to the fibers from the telescope 5 fibers are connected to the MAST calibration unit. The 45 fibers in the assembly have a total length of 5 mm. The feed assembly is mounted on a linear stage to transition between DeepSpec and HighSpec. Bottom: the fiber slit can be moved on a linear stage between one of two positions in order to switch between using DeepSpec and HighSpec. This stage is the only moving part in the design.

Table 2. DeepSpec optical properties

Collimator diameter (mm)	50
Collimator focal length (mm)	150
Camera focal length (mm)	250
u band wavelength range (nm)	365-435
g band wavelength range (nm)	430-540
r band wavelength range (nm)	535-680
i band wavelength range (nm)	670-900
Fiber image size (μm)	42
Peak spectrograph throughput at 550nm (%)	80
typical (dark time + 2.5 magarcsec^{-2}) 10-σ limiting magnitude @ $T_{exp} = 1200$s (AB mag)	20.2
best-case 10-σ limiting magnitude @ $T_{exp} = 1200$s (AB mag)	21.1
Saturation limit @ $T_{exp} = 1200$s (AB mag)	13.5
Saturation limit @ $T_{exp} = 500$s (AB mag)	12.5
Saturation limit @ $T_{exp} = 10$s (AB mag)	8.3

2.4 Dichroic mirrors

DeepSpec uses three dichroic mirrors to split the polychromatic beam to to four beams, each covering a bandpass of ~ 120 nm. The mirrors are manufactured by Asahi Spectra with a $\lambda/8$ flatness, and are a copy of the Son of X-Shooter (SOXS) dichroics (16). At an angle of incidence of 45° they achieve $> 99\%$ ($> 98\%$) reflection (transmission) efficiency across the bandpass. We specify the resulting bands in Table 2.

Table 3. Collimator and Camera lens prescription showing the radius of curvature, the thickness, and the optical glasses used for each surface. As built values for thickness and radius of curvature are provided.

Part	Surface	Material	Manufacturer	Radius of Curvature (mm)	Thickness (mm)	Mechanical Semi-Diameter (mm)
L1 collimator	1	H-FK61	CDGM	Inf	8.97	25.50
L1 collimator	2	H-BAK5	CDGM	-53.68	5.02	25.50
L1 collimator	3	H-FK61	CDGM	63.43	12.98	25.50
L1 collimator	4	Air	-	-73.65	34.59	25.50
L2 collimator	1	F2	Schott	Inf	14.00	28.50
L2 collimator	2	QF50GTI	CDGM	-47.33	4.96	28.50
L2 collimator	3	H-FK61	CDGM	123.79	7.54	28.50
L2 collimator	4	-	-	-	-	28.50
U Camera	1	N-BK7	Schott	133.42	13.04	31.50
U Camera	2	QF50GTI	CDGM	-92.19	7.96	31.50
U Camera	3	-	-	-518.56	-	31.50
G Camera	1	N-BK7	Schott	138.81	12.99	32.00
G Camera	2	F2	Schott	-99.85	8.00	32.00
G Camera	3	-	-	-392.61	-	32.00
R Camera	1	H-ZBAF21	CDGM	99.36	8.05	31.50
R Camera	2	S-FPM4	Ohara	60.40	10.98	31.50
R Camera	3	-	-	Inf	-	31.50
I Camera	1	H-ZF11	CDGM	133.08	6.01	31.50
I Camera	2	H-ZK11	CDGM	57.02	13.47	31.50
I Camera	3	-	-	Inf	-	31.50

2.5 Prisms

The resolution of a spectrograph is given by (17)

$$\mathcal{R} = \frac{\lambda \mathrm{A}}{r\phi} \frac{D_{col}}{D_{tel}}$$

Where A is the angular dispersion, given for a single minimum deviation prism by

$$A = \frac{d\beta}{d\lambda} = \frac{t}{a} \frac{dn}{d\lambda}$$

where t is the base length of the prism and a is the beam width. To identify the preferred prism substrate and apex angle for each band, we calculated the throughput and resolution curves of a minimal dispersion prism with a mean resolution of $\mathcal{R}_{mean} = 650$ for all glasses in the Ohara, Schott and CDGM glass catalogs. A glass was selected for each band based on availability, in order to minimize $\mathcal{R}_{max}/\mathcal{R}_{min}$, and maximize the throughput across the band. We also avoided large angles of incidence which impact the efficiency of anti-reflective coatings. In Fig. 4 we show the resulting resolution curve for a $25\mu m$ image quality. Table 4 summarizes the chosen prism parameters.

2.6 Cameras

The camera optics of each band were required to maintain $< 10\,\mu m$ image quality at all wavelengths. To achieve Nyquist sampling with the 13.3 μm detector pixels, the effective focal length of the cameras was chosen to be in the range 235mm - 250mm, resulting in a magnification of 1.5-1.67, and a fiber core image of 39 μm-42 μm or roughly 3 pixels in diameter. Due to the relatively narrow band, a simple achromat doublet was sufficient to achieve our requirements for all four bands. Total throughput and material availability were considered when

Table 4. Prism properties for the DeepSpec spectrograph

band	Angle of Incidence (deg)	Apex angle (deg)	base length (mm)	Glass type	manufacturer
u	38.0	46.2	58.0	LLF1	Ohara
g	51.9	60.8	94.0	LLF1	Ohara
r	48.7	52.0	77.0	SF1	Schott
i	62.2	62.6	122.5	SF1	Schott

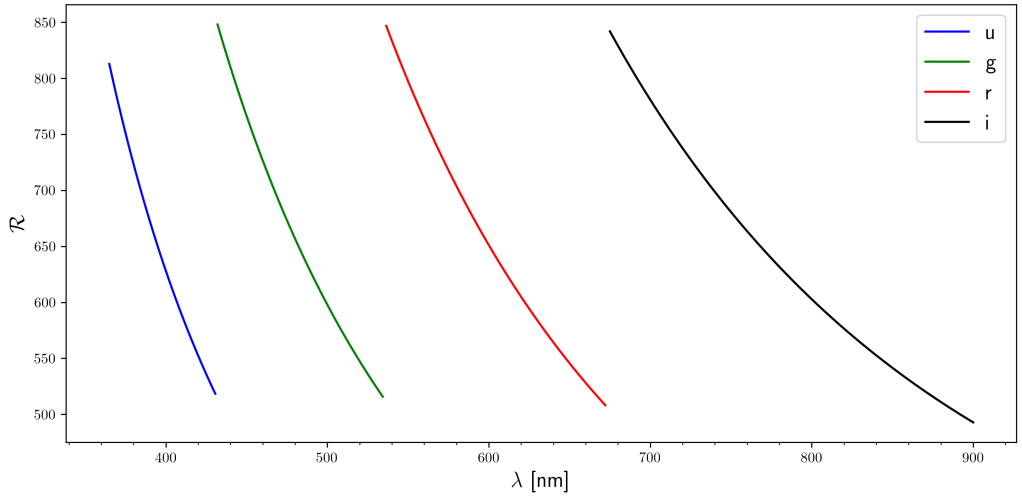

Figure 4. The spectral resolution of DeepSpec as a function of wavelength for a uniform image quality of 25μm

selecting the optical glasses used for each of the lenses. Our chosen camera lens design was found to be insensitive to the expected manufacturing tolerance (equivalent to Optimax precision level tolerance requirements[†]). We provide a full prescription of our camera lenses in Table 3.

2.7 Detectors

Splitting the beam into four bands of ~ 120 nm each allows us to take advantage of modest format CCD cameras. We select four GreatEyes ELSEi MU2 Deep-depletion back-illuminated CCD cameras with E2V CCD47-20 sensors, with a quantum efficiency exceeding 85% between 400 nm and 700 nm. Their properties are summarized in Table 5. The four detectors will be cooled using a 3.6 kW water chiller through a 5-branch manifold to guarantee minimal thermal noise. Each detector is coupled to CS25 shutters from Uniblitz to guarantee precise and uniform exposure times across the detector.

Table 5. CCD parameters

Number of units	20
Pixel size (μm)	13
CCD pixel format	1024×1024
Dark current @ -100C (e^{-1} s^{-1} $pixel^{-1}$)	0.0004
Read noise @ 50,000 pix s^{-1} (e^{-1})	2.9
peak CCD quantum efficiency	95%
Minimum CCD quantum efficiency (400 nm-850 nm)	>85%
Well capacity	120,000 e^-

[†]https://www.optimaxsi.com/charts/manufacturing-tolerance-chart/

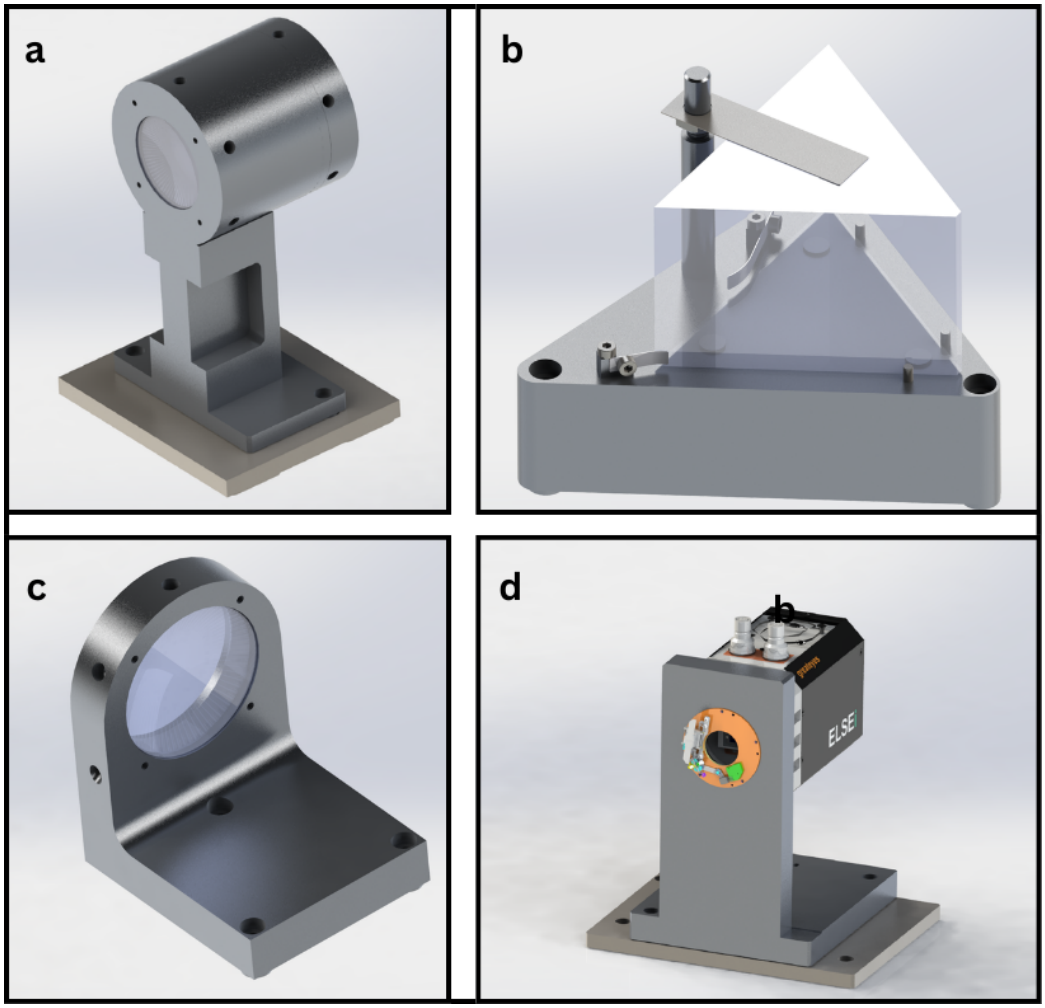

Figure 5. Individual elements of the DeepSpec design with their housing and optical table interface. (a) The 2 collimator triplet lenses are mounted in a single cylinder. (b) The prisms, mounted using a clamping arm. (c) The camera doublet lenses, mounted using a standard cylindrical housing. (d) The detectors, mounted using a fixed mount with a shutter.

3. OPTO-MECHANICAL DESIGN

A dedicated instrument room, in which temperature is stabilized at a level of 1°C, will house all MAST instruments. DeepSpec, as well as its twin HighSpec (8), will be assembled on a dedicated optical table with active vibration isolation. These conditions allow us to adopt a simple mechanical design for the DeepSpec spectrograph, in which optical elements are bonded to Al-6061 mounts using Dowsil 3145 RTV, installed on an aluminum base plate that is coupled to the optical table using semi-kinematic interfaces. The collimator triplets are mounted in a single cylindrical housing, and interface the optical table through a separate base plate. This eases the alignment procedure, as the collimator is aligned independently to the beam diverging from the quasi-slit. The simple semi-kinematic interface between the stainless steel base plate and the aluminum collimator housing will mitigate differences in thermal expansion. The prisms are mounted using a clamping arm, while the dichroic and camera lenses are mounted in standard cylindrical housing. The four DeepSpec CCD detectors are mounted on fixed mounts on separate plates from the rest of the optics, enabling independent corrections of the focus position, if needed. The right panel of Fig. 1 shows a 3D rendering of the opto-mechnical design for DeepSpec, and 5 shows individual elements of the mechanical design.

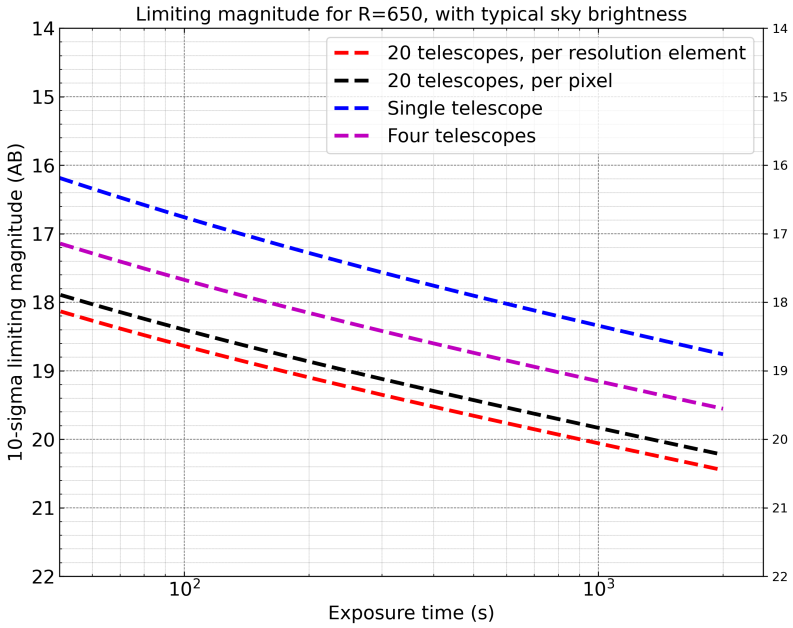

Figure 6. 10-σ limiting magnitude of the MAST array with different telescope configuration with a 2X2 binning, under realistic conditions (dark time + 2.5 mag arcsec^{-2}).

4. EXPECTED PERFORMANCE

4.1 Signal to noise and limiting magnitude

To estimate the SNR, we use the CCD equation (18)

$$\frac{S}{N} = \frac{\varepsilon N_*}{\sqrt{N_* + \left(1 + \frac{n_{pix}}{n_B}\right)\left(N_S + n_{pix}\left[N_D + N_R^2 + G^2\sigma_f^2\right]\right)}}$$

where N_* is the total signal at the entrance of a single telescope, ε is the sky to counts efficiency, n_B is the total number of background pixels used to estimate the mean background, $n_{\rm pix}$ is the number of pixels used to estimate the source, N_s is the total background from a single telescope, N_D is the number dark current electrons, N_R is the number of electrons per pixel from read noise, and G is the gain of the CCD in electrons/ADU and σ_f is the 1-sigma error introduced within the A/D converter. We assume $n_{pix,bkg} = n_{pix,source}$ and compute the SNR per single resolution element and per pixel. All noise terms are considered separately for each imaged trace, such the resulting equation for the SNR from n_{tel} traces will be $\frac{S}{N}_{total} = \sqrt{(n_tel)}\frac{S}{N}_{single}$. In Fig. 6 we show the 10 σ limiting magnitude for different telescope groupings, calculated at realistic conditions for WAO (18.4 mag arcsec^{-2}, corresponding to 2.5 magnitudes brighter than dark time). We assume 85% mirror reflectivity (the minimum reflectivity in the 400nm-700nm band required from PlaneWave). For the fiber losses, we account for 6% loss due to FRD and 8% due to reflection losses at the entrance and exit from the fiber. Additional losses related seeing are expected to be small, as the projected fibers size is $\sim 2\farcs5 - 2\farcs9$ ″, significantly larger than the typical median seeing disk FWHM of $1\farcs4$, and marginally better than the 95 seeing percentile of $2\farcs36$ (3). This margin with respect to the typical seeing includes room for guiding and tracking errors. Wavelength-dependent fiber transmission losses are estimated for a 20 m fiber length based on similar broad spectrum fibers, and the typical distance of the telescopes from the instrument room.

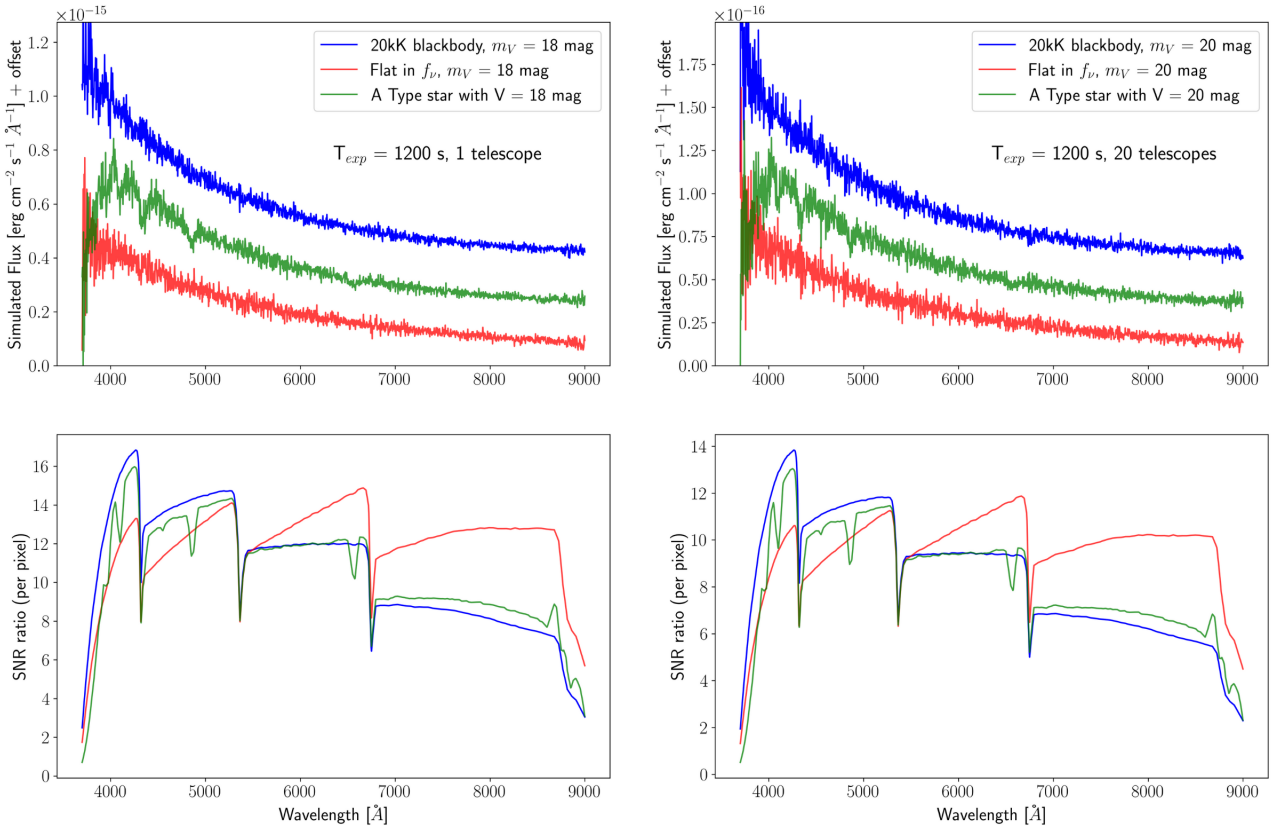

Figure 7. Simulated spectra of a thermal source and a flat in f_ν source, and an A Type star normalized to a V band brightness of 20 mag (left) and 18 mag (right). In order to minimize the dead time of the telescope, the number of telescopes can be adjusted instead of exposure time.

4.2 Observing modes

DeepSpec is a highly versatile and flexible instrument. Due to the lack of pointing restrictions on the MAST telescopes other than airmass$>$ 2 and the ability to image traces separately on the CCD, MAST can observe either a single target with all 20 telescopes, or multiple targets simultaneously with a subset of telescopes for each target. When observing targets brighter than the limiting magnitude for a given exposure time, it is advisable to reduce the number of telescopes rather than the exposure time. This is due to 2 main reasons:

1. Due to the multiple number of traces, read noise accounts for a significant fraction in the noise budget. Background limited performance is achieved for faint targets at longer exposures. The right panel of Fig. 8 shows the contribution of different noise terms to the total exposure variance from a sum of 20 traces. At a binning of 2X2 (1X1), the background variance term will be equal to the read noise variance term at an exposure time of 250 s (1000 s). The read noise contribution will thus be negligible only if the appropriate binning is used, and at exposure times of $> 1000\,s$, unless the target is very bright compare to the limiting magnitude.

2. Typically, dead-time due to slewing and acquisition limits the spectrograph efficiency in terms of spectra/hour. In DeepSpec, Overhead time can be parallelized when observing with multiple telescopes. As we will show below, a higher number of spectra/hr is possible for the same SNR if a parallel strategy is enforced.

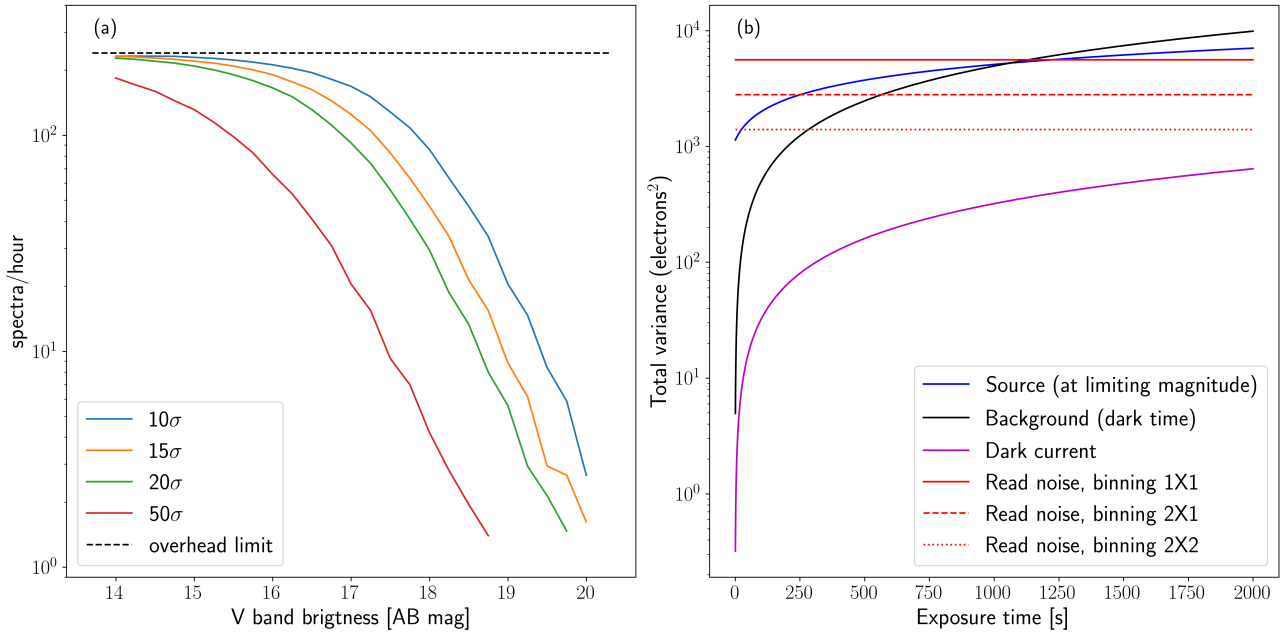

Figure 8. (a) Number of spectra per hour as a function of target brightness that MAST/DeepSpec can observe for different SNR requirements, assuming a 5 min overhead for slewing and acquisition. (b) Contribution of background, source, dark current and read noise noise terms to the total variance as a function of exposure time, for the summed spectrum from 20 traces. We show read noise terms under different binning configurations. The source is assumed to be at the 10σ limiting magnitude corresponding to the exposure time.

To illustrate these properties, we simulated spectral response for an A-type star, a 20 K blackbody, and a flat spectrum, see Fig. 7. We simulate spectra for a V band brightness of 18 mag and 20 mag with a fixed exposure time of 1200 s. By varying the number of telescopes instead of exposure time, we achieve a similar SNR for all cases. The example shown in Fig. 7 illustrates the effectiveness of our approach. By observing an ensemble of targets of a similar brightness using the maximal exposure time and minimal number of telescopes, we reduce the fraction of dead-time and the total number of traces (thus reducing read-noise). We calculate the number of spectra per hour that can be observed using this strategy. In Fig. 8 we show the number of spectra per hour DeepSpec can observe for different SNR requirements as a function of target brightness, assuming a 5 min overhead for slewing and acquisition. Our results indicate that DeepSpec will be especially powerful for the study of transient demographics. In the $17-19$ mag range, DeepSpec can observe tens of targets per hour. This allows a statistically complete spectroscopic time-series of transients sampled throughout their evolution at near peak brightness. Since its inception, the ZTF bright transient survey (BTS) has classified over 5000 supernovae brighter than 19 mag (19), allowing to study supernovae demographics in an unbiased way. However, the BTS has relied on many low SNR spectra, non-uniform sampling, a typical spectral resolution of $\mathcal{R}\sim$100, and requires a minimum of a single spectrum per supernovae for classification. A DeepSpec based survey probing the demographics of transients at different phases would significantly improve upon the BTS. Such a survey would allow, for example, to calculate the fraction of recently observed type switching supernovae (20), and more generally classify supernovae based on their spectro-temporal evolution rather than a single spectrum (21). If compelling targets require spectroscopic coverage at early times or in the nebular phase, spectra can be acquired with more telescopes. In the bright end (<16 mag), DeepSpec can observe hundreds of spectra per hour with very high SNR (~ 50). This is ideal for spectral surveys of volume limited stellar samples, as well as phase-resolved spectroscopic time-series for variable stars. Other possible modes of operation include staring with a single telescope at a bright target for continuous monitoring. For a typical exposure time of 1200s for faint targets, this can be done at minimal SNR loss for targets as bright as 13.5 mag with no risk of saturation.

5. SUMMARY

In this paper, we presented the optical and opto-mechanical design of the low-resolution DeepSpec spectrograph for the Multi Aperture Spectroscopic Telescope array. Our simple four-band design has a minimal number of optical element and is optimized for high throughput while achieving the desired image quality across the field of view and bandpass, resulting in a high end-to-end efficiency of $> 65\%$. By imaging the traces from different fibers separately on the detector, we maintain the ability to multiplex targets or observe a single target with all telescopes simultaneously, summing the spectral traces after data processing. This feature of the optical design enables DeepSpec to either act as a flexible multi-object or single object spectrograph. We achieve background limited performance when summing 20 traces at the faint source limit with a 15 minute exposure. In the bright end, spectrograph efficiency in terms of spectra per unit time is significantly improved compared to long-slit spectrographs due to time saved on slewing and acquisition. Compared to other multi-object spectrographs, DeepSpec coupled to MAST is not limited to multiplexing observations over a single field of view - making it ideal for targeted follow-up of a large number of targets for a single science case. DeepSpec is ideally suited for following up faint transients, time-series studies of both transients and variable sources, and for filtering through large samples of stellar objects brighter than 17 mag. DeepSpec is currently in the assembly, integration, and testing phase, and will be coupled to the MAST array towards the end of 2024.

ACKNOWLEDGMENTS

S.B.A. is grateful for support from the Azrieli Foundation, André Deloro Institute for Advanced Research in Space and Optics, Peter and Patricia Gruber Award, Willner Family Leadership Institute for the Weizmann Institute of Science, Aryeh and Ido Dissentshik Career Development Chair, Israel Science Foundation, Israel Ministry of Science, and Minerva Stiftung. A.G-Y.'s research is supported by the EU via ERC grant 725161, the ISF GW excellence center, an IMOS space infrastructure grant and BSF/Transformative and GIF grants, as well as the André Deloro Institute for Advanced Research in Space and Optics, The Helen Kimmel Center for Planetary Science, the Schwartz/Reisman Collaborative Science Program and the Norman E Alexander Family Foundation ULTRASAT Data Center Fund, Minerva and Yeda-Sela; A.G.-Y. is the incumbent of the Arlyn Imberman Professorial Chair. E.O.O. is grateful for the support of grants from the Willner Family Leadership Institute, André Deloro Institute, Paul and Tina Gardner, The Norman E Alexander Family M Foundation ULTRASAT Data Center Fund, Israel Science Foundation, Israeli Ministry of Science, Minerva, NSF-BSF, Israel Council for Higher Education (VATAT), Sagol Weizmann-MIT, Yeda-Sela, and the Rosa and Emilio Segre Research Award. This research was supported by the Institute for Environmental Sustainability (IES) and The André Deloro Institute for Space and Optics Research at the Weizmann Institute of Science. H.K. was funded by the Research Council of Finland projects 324504, 328898, and 353019.

References

[1] Bellm, E. C., Kulkarni, S. R., Graham, M. J., et al., "The Zwicky Transient Facility: System Overview, Performance, and First Results," *Publications of the Astronomical Society of the Pacific* **131**, 018002 (2019).

[2] Shvartzvald, Y., Waxman, E., Gal-Yam, A., et al., "ULTRASAT: A Wide-field Time-domain UV Space Telescope," *ApJ* **964**(1), 74 (2024).

[3] Ofek, E. O., Ben-Ami, S., Polishook, D., et al., "The Large Array Survey Telescope-System Overview and Performances," *Publications of the Astronomical Society of the Pacific* **135**, 065001 (2023).

[4] Bruch, R. J., Gal-Yam, A., Schulze, S., et al., "A Large Fraction of Hydrogen-rich Supernova Progenitors Experience Elevated Mass Loss Shortly Prior to Explosion," *ApJ* **912**, 46 (2021).

[5] Blagorodnova, N., Neill, J. D., Walters, R., et al., "The SED Machine: A Robotic Spectrograph for Fast Transient Classification," *PASP* **130**, 035003 (2018).

[6] Ofek, E. O. and Ben-Ami, S., "Seeing-limited Imaging Sky Surveys—Small versus Large Telescopes," *PASP* **132**, 125004 (2020).

[7] Sofer Rimalt, Y., Ben Ami, S., Mazeh, T., et al., "HighSpec: a novel high-resolution narrow band-pass spectrograph," in [*Ground-based and Airborne Instrumentation for Astronomy IX*], Evans, C. J., Bryant, J. J., and Motohara, K., eds., *Society of Photo-Optical Instrumentation Engineers (SPIE) Conference Series* **12184**, 1218459 (2022).

[8] Sofer Rimalt, Y., Ben Ami, S., Ofek, E., et al., "HighSpec: high-resolution spectrograph for the MAST telescope array," in [*Ground-based and Airborne Instrumentation for Astronomy X*], *Society of Photo-Optical Instrumentation Engineers (SPIE) Conference Series* **13069**, (2024).

[9] Kuncarayakti, H., Achren, J., Ben Ami, S., et al., "Calibration unit design for the Multi- Aperture Spectroscopic Telescope (MAST)," in [*Ground-based and Airborne Instrumentation for Astronomy X*], *Society of Photo-Optical Instrumentation Engineers (SPIE) Conference Series* **13069**, (2024).

[10] Gal-Yam, A., Bruch, R., Schulze, S., et al., "A WC/WO star exploding within an expanding carbon-oxygen-neon nebula," *Nature* **601**, 201–204 (2022).

[11] Perley, D. A., Sollerman, J., Schulze, S., et al., "The Type Icn SN 2021csp: Implications for the Origins of the Fastest Supernovae and the Fates of Wolf-Rayet Stars," *ApJ* **927**(2), 180 (2022).

[12] Irani, I., Chen, P., Morag, J., et al., "SN 2022oqm–A Ca-rich Explosion of a Compact Progenitor Embedded in C/O Circumstellar Material," *ApJ* **962**(2), 109 (2024).

[13] De, K., Kasliwal, M. M., Tzanidakis, A., et al., "The Zwicky Transient Facility Census of the Local Universe. I. Systematic Search for Calcium-rich Gap Transients Reveals Three Related Spectroscopic Subclasses," *ApJ* **905**(1), 58 (2020).

[14] Manser, C. J., Gänsicke, B. T., Gentile Fusillo, N. P., et al., "The frequency of gaseous debris discs around white dwarfs," *MNRAS* **493**(2), 2127–2139 (2020).

[15] Jiang, H., Hu, Z., Xu, M. , et al., "The preliminary design of the next generation Palomar spectrograph for 200-inch Hale telescope," in [*Ground-based and Airborne Instrumentation for Astronomy VII*], Evans, C. J., Simard, L., and Takami, H., eds., *Society of Photo-Optical Instrumentation Engineers (SPIE) Conference Series* **10702**, 107022L (2018).

[16] Rubin, A., Ben-Ami, S., Hershko, O., et al., "Progress on the UV-VIS arm of SOXS," in [*Ground-based and Airborne Instrumentation for Astronomy VIII*], Evans, C. J., Bryant, J. J., and Motohara, K., eds., *Society of Photo-Optical Instrumentation Engineers (SPIE) Conference Series* **11447**, 114475L (2020).

[17] Schroeder, D. J., "Chapter 12, astronomical optics (second edition)," 304–320, Academic Press, San Diego, second edition ed. (2000).

[18] Howell, S. B., [*Handbook of CCD Astronomy*], Cambridge University Press (2000).

[19] Perley, D. A., Fremling, C., Sollerman, J. , et al., "The Zwicky Transient Facility Bright Transient Survey. II. A Public Statistical Sample for Exploring Supernova Demographics," *ApJ* **904**, 35 (2020).

[20] Sharma, Y., Sollerman, J., Kulkarni, S. R., et al., "Dramatic Rebrightening of the Type-changing Stripped-envelope Supernova SN 2023aew," *ApJ* **966**, 199 (2024).

[21] Bengyat, O. and Gal-Yam, A., "Characterization of Supernovae Based on the Spectral-Temporal Energy Distribution: Two Possible SN Ib Subtypes," *ApJ* **930**, 31 (2022).